


# Effect of Resonant Aggregate Parameters in Metaconcrete Thin Plates on Flexural Bandgaps: Numerical Simulations

André Luiz Louzeiro Carvalho<sup>a</sup>, Cássio Bruno Florêncio Gomes<sup>a</sup>, José Maria Campos dos Santos<sup>b</sup>,  
Edson Jansen Pedrosa de Miranda Jr.<sup>a,c,d,\*</sup> 

<sup>a</sup>Instituto Federal do Maranhão (IFMA), Programa de Pós-Graduação em Engenharia de Materiais (PPGEM), Avenida Getúlio Vargas, 4, 65030-005, São Luís, MA, Brasil.

<sup>b</sup>Universidade Estadual de Campinas (UNICAMP), Faculdade de Engenharia Mecânica (FEM), Departamento de Mecânica Computacional (DMC), Rua Mendeleev, 200, 13083-970, Campinas, SP, Brasil.

<sup>c</sup>Instituto Federal do Maranhão (IFMA), Extensão Itaqui Bacanga (EIB), Departamento de Ensino (DE), Rua Afonso Pena, 174, 65010-030, São Luís, MA, Brasil.

<sup>d</sup>Instituto Tecnológico Vale (ITV), Rua Professor Paulo Magalhães Gomes, Bauxita, 35400-000, Ouro Preto, MG, Brasil.

Received: December 14, 2022; Revised: May 17, 2023; Accepted: October 20, 2023

Plate structures are widely used in civil engineering, for instance, as slabs, foundations, and retaining walls. In structural acoustics, flexural wave control becomes an important parameter for the safety of engineering thin structures. Metaconcrete is a new type of concrete where conventional aggregates are replaced by resonant aggregates, made of a solid core coated with a compliant material, which presents wave attenuation properties. Hence, the aim of this paper is to evaluate the band structure of flexural waves in a metaconcrete, using the thin plate theory associated with the improved plane wave expansion (IPWE) method. The effect of aggregate geometry, core density, Young's modulus of the coating, and number of layers are analyzed. Complete bandgaps are observed for almost all inclusions. The results reveal the possibility of adjusting the desired frequency range according to the configuration of the resonators for flexural vibration management through metaconcrete thin plates.

**Keywords:** *elastic metamaterial, resonant inclusions, multilayered resonators, thin plate theory, Fourier series expansion.*

## 1. Introduction

Photonic crystals are artificial materials in a periodic array with differing dielectric constants, creating a light filtering behavior in certain directions with specified frequencies, termed as photonic bandgap, if the dielectric constants of the materials are sufficiently different<sup>1</sup>. Similarly to the photonic crystals, phononic crystals have been proposed. They are artificial periodic composite materials consisting of periodically distributed inclusions in a matrix with elastic property contrast, which can yield phononic bandgap, preventing the propagation of acoustic or elastic waves<sup>2</sup>. The phononic and photonic bandgaps arise from the nature of the constituents, the contrast between the physical properties of the resonators and matrix, and the structural geometry<sup>3</sup>, and are physically originated from Bragg and Mie resonances through wave scattering<sup>2,3</sup>. Since phononic crystals are based on the Bragg's scattering mechanism, its design is limited by spatial periodicity, given that the incident wavelength is comparable to the unit cell size of these structures, thus, for audible frequency, in meter scale, the use of Bragg gaps is untenable for filtering acoustic waves<sup>4</sup>. To cope with this issue, Liu et al.<sup>5</sup> introduced the local resonance mechanism, reified in a locally resonant structure, a composite containing

lead balls coated with a thin layer of silicone rubber spatially arranged in an epoxy matrix, also known as sonic crystal or mechanical metamaterial. Bandgaps are opened up in two orders of magnitude smaller than the incoming wavelength when the material interacts with a wave, induced by inclusions, arising even in absence of periodicity.

Mechanical metamaterials are a new category of materials with counterintuitive properties, *e.g.*, negative density and stiffness<sup>6</sup>, negative<sup>7</sup> or zero<sup>8</sup> Poisson's ratio, programmable behavior<sup>9</sup>, perfect isolation vibration<sup>10</sup>, non-reciprocity systems<sup>11</sup>, and so forth. Recently, the metamaterial concept has been introduced in concrete, the main material used in civil engineering, firstly proposed by Mitchell et al.<sup>12</sup>, termed as metaconcrete, where engineered aggregates, consisting of metal core encapsulated in a polymer layer, replace sand and gravel aggregates. In this model, resonators resemble a mass-spring system, in which the coating is simplified as a spring, with a linear stiffness constant, the rigid core of mass, and the mortar matrix is equivalent a rigid body having a certain mass. When a force with frequency close to natural frequency of resonators is applied, inclusions constrain a portion of the supplied energy and activate bandgaps, weakening the motion of the elastic waves<sup>13</sup>.

Numerical studies have been carried out demonstrating the reduction for both longitudinal and transverse vibration modes of metaconcrete<sup>12-19</sup>, in addition to experimental

\*e-mail: [edson.jansen@ifma.edu.br](mailto:edson.jansen@ifma.edu.br)

validations endorsing this behavior<sup>20,22</sup>, even if the inclusions are dispersed in a random<sup>23,24</sup> or quasi-random arrangement<sup>25</sup>. Furthermore, a simplified analytical model for metaconcrete filled with randomly distributed resonators has been proposed<sup>26</sup>. Multilayered engineered aggregates have been also investigated numerically and experimentally<sup>27</sup>.

Flexural vibrations of thin structures are mainly responsible to the sound radiation and structural damage, for which they deserve careful attention in civil engineering<sup>28</sup>. The ability of thin plates to absorb and suppress flexural waves by creating bandgaps has been assessed numerically and experimentally, in which contrast of the constituents plays a fundamental role for the variation of the bandgap width<sup>29-32</sup>. Regarding metaconcrete, Miranda Jr. et al.<sup>33</sup> proposed that thin plates can be applied to control flexural vibration in low frequencies, hence, this new composite can be used to optimize the safety and stability of continuous structures.

In this work, we are concerned with the investigation of an isotropic thin plate of metaconcrete, varying the parameters of resonators, *i.e.*, core diameter, coating thickness, core density, coating stiffness, and number of materials layers, applying Kirchhoff-Love plate theory and 2-D models. The influence of these variations on the flexural band structure was analyzed by using the improved plane wave expansion (IPWE) method. Metaconcrete thin plate was composed by metallic cylindrical cores coated with polymeric material arranged in a square array embedded in a mortar matrix. The results reveal that the width and location of the bandgaps are strongly related to the diameter and density of the core, the thickness and stiffness of the coating, the contrast of the elastic parameters of the resonator materials, and the number of layers. In addition, the formation of flatbands depends on the coating thickness.

## 2. Improved Plane Wave Expansion Method

### 2.1. Formulation of the method

In this section, the IPWE formulation for the Kirchhoff-Love plate theory is presented. We consider wave propagation limited to  $xy$  plane, finite thickness, 2-D periodicity, and isotropy. IPWE method has high efficiency, easy implementation, and low computational cost in comparison to other methods, introducing simplicity and feasibility to complex problems, especially in case of high material properties mismatch in order to get a good convergence<sup>34,35</sup>. In this investigation, microstructural effects are discarded, since here we applied the linear elasticity theory and a simpler thin-plate model of continuum mechanics. In the Kirchhoff-Love plate theory, the hypotheses yield to the formulation that governs the flexural vibration of a plate, described as:

$$\begin{aligned} -\alpha \frac{\partial^2 \mathbf{u}_z}{\partial t^2} &= \frac{\partial^2}{\partial x^2} \left( D \frac{\partial^2 \mathbf{u}_z}{\partial x^2} + \beta \frac{\partial^2 \mathbf{u}_z}{\partial y^2} \right) \\ + 2 \frac{\partial^2}{\partial x \partial y} \left( \gamma \frac{\partial^2 \mathbf{u}_z}{\partial x \partial y} \right) &+ \frac{\partial^2}{\partial y^2} \left( D \frac{\partial^2 \mathbf{u}_z}{\partial y^2} + \beta \frac{\partial^2 \mathbf{u}_z}{\partial x^2} \right), \end{aligned} \quad (1)$$

where  $\mathbf{u}_z$  is the transverse displacement vector,  $D = \frac{Eh^3}{12(1-\nu^2)}$  is the flexural rigidity,  $E$  is the Young's modulus,  $\nu$  is the

Poisson's ratio,  $\alpha = \rho h$ , with  $\rho$  being the mass density and  $h$  the thickness plate,  $\beta = D\nu$ , and  $\gamma = D(1-\nu)$ . All of these parameters are periodic functions of the position vector  $\mathbf{r} = (x, y)$ .

Regarding the periodic nature of these quantities, it is possible to apply the Floquet-Bloch theorem to the displacement, and to expand the amplitude of the displacement and properties using a spatial Fourier series, respectively:

$$\mathbf{u}_z(\mathbf{r}) = \sum_{\mathbf{G}_1} \mathbf{u}_{\mathbf{k}}(\mathbf{G}_1) e^{i(\mathbf{k}+\mathbf{G}_1)\cdot\mathbf{r}}, \quad (2)$$

$$p(\mathbf{r}) = \sum_{\mathbf{G}_2} p(\mathbf{G}_2) e^{i\mathbf{G}_2\cdot\mathbf{r}}, \quad (3)$$

where  $\mathbf{k}$  is the Bloch wave vector, also known as wavenumber,  $\mathbf{u}_{\mathbf{k}}(\mathbf{G}_1)$  and  $p(\mathbf{G}_2)$  represents the Fourier coefficients of the displacement and properties, respectively, while  $\mathbf{G}_1$  and  $\mathbf{G}_2$  are the reciprocal lattice vectors for the square lattice.

Substituting Equations 2 and 3 in Equation 1, considering  $\mathbf{G}_3 = \mathbf{G}_1 + \mathbf{G}_2$ , multiplying by  $\frac{1}{a} e^{-i(\mathbf{k}+\mathbf{G}_3)\cdot\mathbf{r}}$  and integrating over the area occupied by the individuals in the unit cell, one can write the corresponding eigenvalue problem  $\omega(\mathbf{k})$ :

$$\begin{aligned} \sum_{\mathbf{G}_1=-\infty}^{+\infty} &\left[ -\omega^2 \alpha (\mathbf{G}_3 - \mathbf{G}_1) + \left[ \frac{1}{D(\mathbf{G}_3 - \mathbf{G}_1)} \right]^{-1} (\mathbf{k} + \mathbf{G}_1)_x^2 (\mathbf{k} + \mathbf{G}_3)_x^2 \right. \\ &\quad \left. + \left[ \frac{1}{\beta(\mathbf{G}_3 - \mathbf{G}_1)} \right]^{-1} (\mathbf{k} + \mathbf{G}_1)_y^2 (\mathbf{k} + \mathbf{G}_3)_y^2 \right. \\ &+ 2 \left[ \frac{1}{\gamma(\mathbf{G}_3 - \mathbf{G}_1)} \right]^{-1} (\mathbf{k} + \mathbf{G}_1)_x (\mathbf{k} + \mathbf{G}_1)_y (\mathbf{k} + \mathbf{G}_3)_x (\mathbf{k} + \mathbf{G}_3)_y \\ &\quad \left. + \left[ \frac{1}{D(\mathbf{G}_3 - \mathbf{G}_1)} \right]^{-1} (\mathbf{k} + \mathbf{G}_1)_y^2 (\mathbf{k} + \mathbf{G}_3)_y^2 \right. \\ &\quad \left. + \left[ \frac{1}{\beta(\mathbf{G}_3 - \mathbf{G}_1)} \right]^{-1} (\mathbf{k} + \mathbf{G}_1)_x^2 (\mathbf{k} + \mathbf{G}_3)_x^2 \right] \mathbf{u}_{\mathbf{k}}(\mathbf{G}_1) = 0, \end{aligned} \quad (4)$$

where, for instance,  $\left[ \frac{1}{p(\mathbf{G}_3 - \mathbf{G}_1)} \right]^{-1}$  represents the inverse of the Toeplitz matrix  $\left[ \frac{1}{p(\mathbf{G}_3 - \mathbf{G}_1)} \right]$ . Equation 4 denotes an infinite sum of equations, therefore, one must truncate Fourier series, restricting vector components to the  $[-M_{\max}, M_{\max}]$ , resulting in a total of  $(2M+1)^N$  plane waves, where  $N$  is equivalent to the dimension of the system, here, a 2-D model, thus  $N=2$ .

Since the symmetry of the irreducible Brillouin zone (IBZ) in the first Brillouin zone (FBZ), a usual procedure is to analyze the Bloch wave vector in the contour of the IBZ in order to calculate the band structure<sup>35</sup>. IBZ points in Figure 1 for square lattice are  $\Gamma(0, 0)$ ,  $X(\pi/L, 0)$ , and  $M(\pi/L, \pi/L)$ , where  $L$  is the lattice constant for square unit cell.

### 2.2. Application and validation of the algorithm

In order to verify the effect of inclusion parameters on the flexural bandgaps, we conducted a numerical study with a metaconcrete thin plate. The dispersion relations were calculated applying the IPWE method, using 625 plane waves, based on convergence tests. To calibrate the procedure, a recent investigation of a band structure of a metaconcrete thin plate

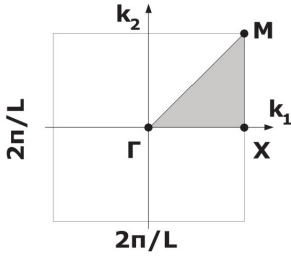


Figure 1. Irreducible Brillouin zone for a square lattice.

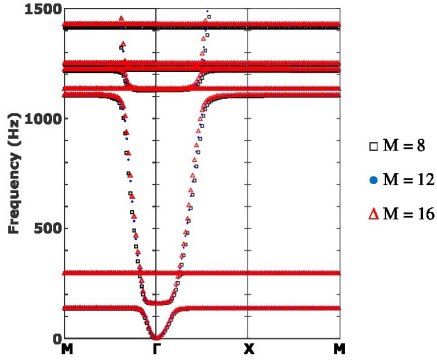


Figure 2. Convergence tests with different number of plane waves.

containing circular bi-layer inclusions reported in Miranda Jr. et al.<sup>33</sup> was used.

Figure 2 shows that small differences appear when  $M$  is varied from 12 to 16. Since the data processing time raises from 6 to 35 minutes with increasing value of  $M$ , we fixed a total of 625 plane waves,  $(2M + 1)^2$ , i.e.,  $M=12$ , based on the computational costs.

### 3. Numerical Results and Discussion

In this section, two different groups of metaconcrete thin plates are displayed, containing circular rods embedded in a mortar matrix, differing by the number of layers, namely, single and multilayer, as illustrated in Figure 3. The single-layer resonator (Figure 3a) is composed by a metallic core (light gray) coated with a polymeric material (white region), while the multilayer aggregate (Figure 3b) uses the former resonator as a base to which two new layers are added, having two metallic layers (light gray) and two polymeric layers (white regions) interspersed.

Generally, a plate is considered thin if the thickness is less than or equal to 10% of the lattice constant<sup>36</sup>. For both cases, we considered a lattice constant of 30 mm and a thickness of 3 mm and limited the investigation up to 20 kHz, except in some configurations.

The material properties are detailed in Table 1. These materials are widely used in engineering. Granite is an intrusive

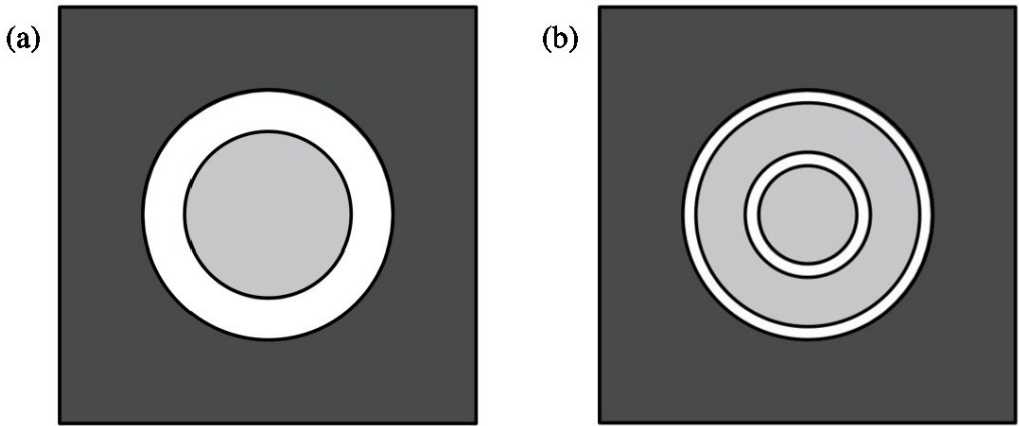


Figure 3. Illustration of a unit cell of a single resonator (a) and multilayer resonator (b).

Table 1. Material properties used in the simulations.

Material	Mass density (kg/m <sup>3</sup> )	Young's modulus (GPa)	Poisson's ratio
C30 Concrete <sup>37</sup>	2,500	30	0.20
Aluminum <sup>38</sup>	2,730	77.6	0.35
A36 Steel <sup>19</sup>	7,800	210	0.30
Copper <sup>39</sup>	8,950	117	0.34
Lead <sup>14</sup>	11,300	16	0.44
Silicone <sup>12</sup>	1,100	0.001	0.47
Natural rubber <sup>12</sup>	900	0.01	0.49
Low density polyethylene (LDPE) <sup>19</sup>	1,100	0.100	0.45
Nylon <sup>14</sup>	1,150	1	0.40
Granite <sup>40</sup>	2,700	34	0.28

igneous rock utilized as coarse aggregate for concrete, here used to evaluate the dispersion relation of regular concrete.

### 3.1 Metaconcrete containing single-layer resonators

#### 3.1.1. Study of geometric parameters

##### 3.1.1.1. Effect of core diameter

For this numerical investigation, the total diameter of the resonator ( $d + 2t$ ), where  $d$  is the core diameter and  $t$  is the layer thickness) changes from 10 mm to 19 mm (*i.e.*, the granulometry of coarse aggregates used in casting of concrete slabs, beams, and columns)<sup>40</sup>. Initially, the coating thickness ( $t$ ) remains at 1 mm. Four core diameters ( $d$ ) of 8 mm (D1), 11 mm (D2), 14 mm (D3), and 17 mm (D4) mm were chosen to investigate the effect of core size on the flexural bandgaps. The considered geometric parameters are given in Table 2.

Furthermore, two additional cases are studied, an ordinary concrete thin plate and a concrete thin plate containing uncoated steel inclusion. For both cases, the maximum resonator size was considered, *i.e.*, 19 mm.

Firstly, the dispersion relation for an ordinary concrete thin plate is visualized in Figure 4a. The plot shows that no bandgaps are opened up until 100 kHz, therefore, ordinary concrete does not have the ability to reduce vibration of flexural waves through resonance and Bragg scattering mechanisms in a wide frequency range. We can see that

by changing the granite for steel (Figure 4b) three partial bandgaps (since they do not entirely cross the IBZ) in the  $\Gamma$ -X (one gap) and X-M (two gaps) directions are opened up, defined by red rectangles, in the frequency ranges from 5.23 to 6.34 kHz, 31.54 to 32.21 kHz, and 60.89 to 63.41 kHz. Given that the formation of bandgaps raises from the contrast between the material constants<sup>34</sup> (only Bragg scattering mechanism in this case), their absence in ordinary concrete can be explained due to the elastic parameters of the materials in the system are insufficiently different, especially the mass density and Young's modulus.

Hereinafter, we discuss the main cases of this study. The band structure as a function of the core size is shown in Figure 5. From Figure 5a, one can observe that the addition of a thin silicone layer (D1) opens up a bandgap (marked by the green rectangle) with frequency ranging from 4.05 to 4.80 kHz. Since this bandgap extends to the entire IBZ, it is known as complete or absolute. This effect arises from the introduction of a softer material than the other two phases (mortar and rigid core), which optimizes the energy transfer between them<sup>12</sup>. As the core diameter increases to 11 mm (Figure 5b, *i.e.*, D2), the complete bandgap widens and shifts to lower frequencies, between 3.39 and 4.37 kHz. Since the unit cell size and coating thickness are kept constant, for the increase in the core mass, the matrix mass must necessarily drop, thus, increasing the mass contrast ratio between the inclusions and matrix, broadening the region of negative effective mass density or bandgap region<sup>16</sup>.

**Table 2.** Resonator geometric data for effect of core size.

ID	Core material	Coating material	Coating thickness (mm)	Core diameter (mm)	Resonator diameter (mm)
D1				8	10
D2	Steel	Silicone	1	11	13
D3				14	16
D4				17	19

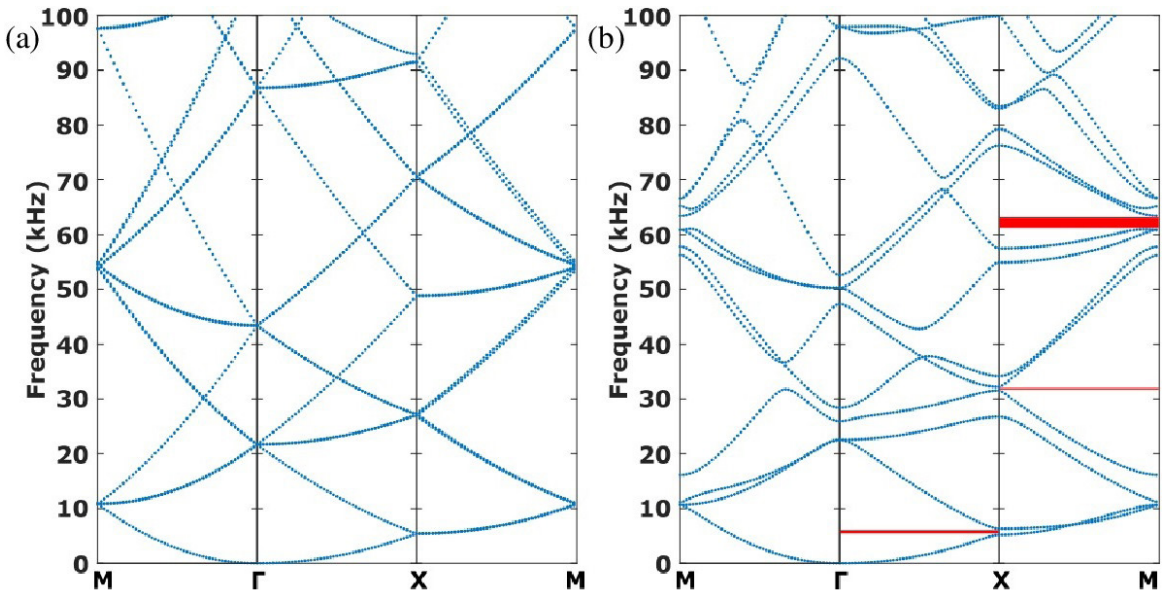


**Figure 4.** Dispersion relation of a thin plate of ordinary concrete (a), concrete containing uncoated steel inclusion (b).

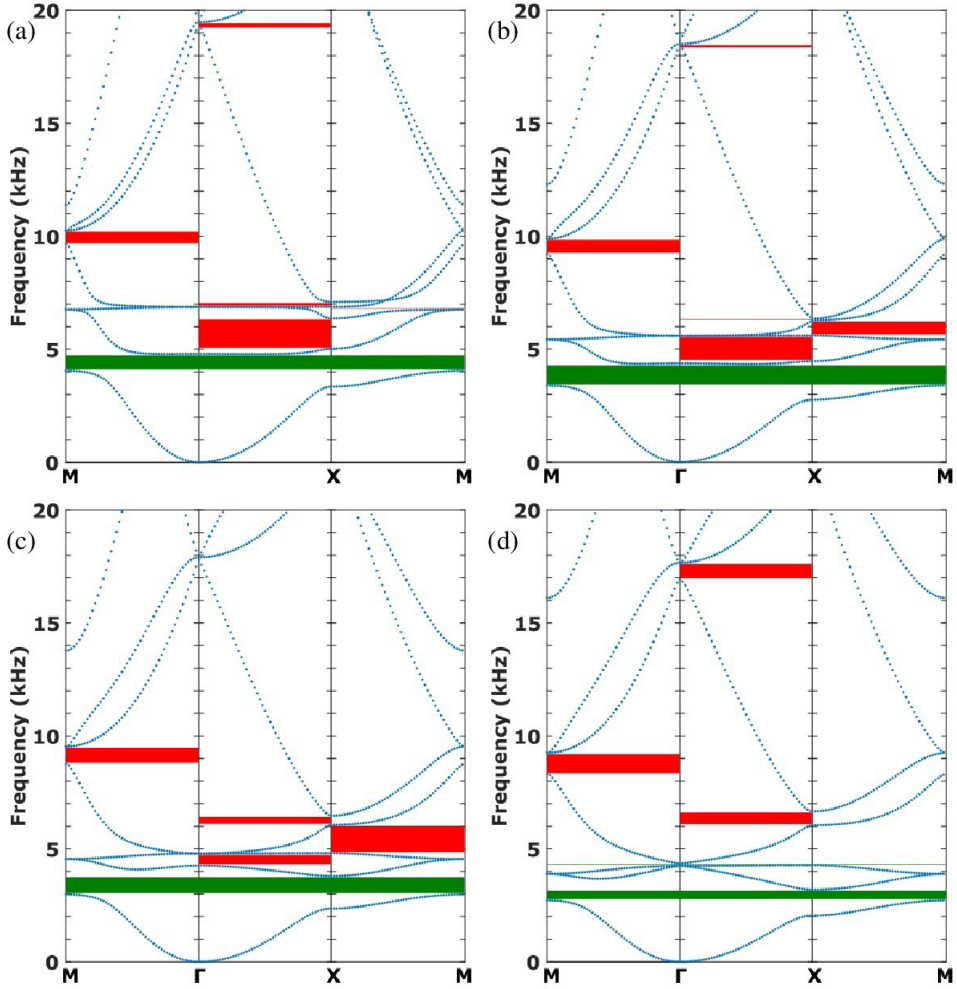


**Figure 5.** Dispersion relation of a thin plate of metaconcrete containing steel resonators coated with silicone in configuration D1 (a), D2 (b), D3 (c), and D4 (d).

With a further increase in the core diameter (Figures 5c and 5d, D3, and D4 configurations, respectively), the complete bandgap tends to shift towards lower frequencies, narrowing bandwidth (with frequency ranging from 2.98 to 3.80 kHz and 2.72 to 3.20 kHz, respectively). Moreover, in D4 configuration (Figure 5d), a second narrow complete bandgap appears in the frequency range between 4.24 and 4.36 kHz, indicating that, as the core diameter increases, a portion of the energy required to open up the first absolute bandgap transfers to higher frequencies.

### 3.1.1.2. Effect of coating thickness

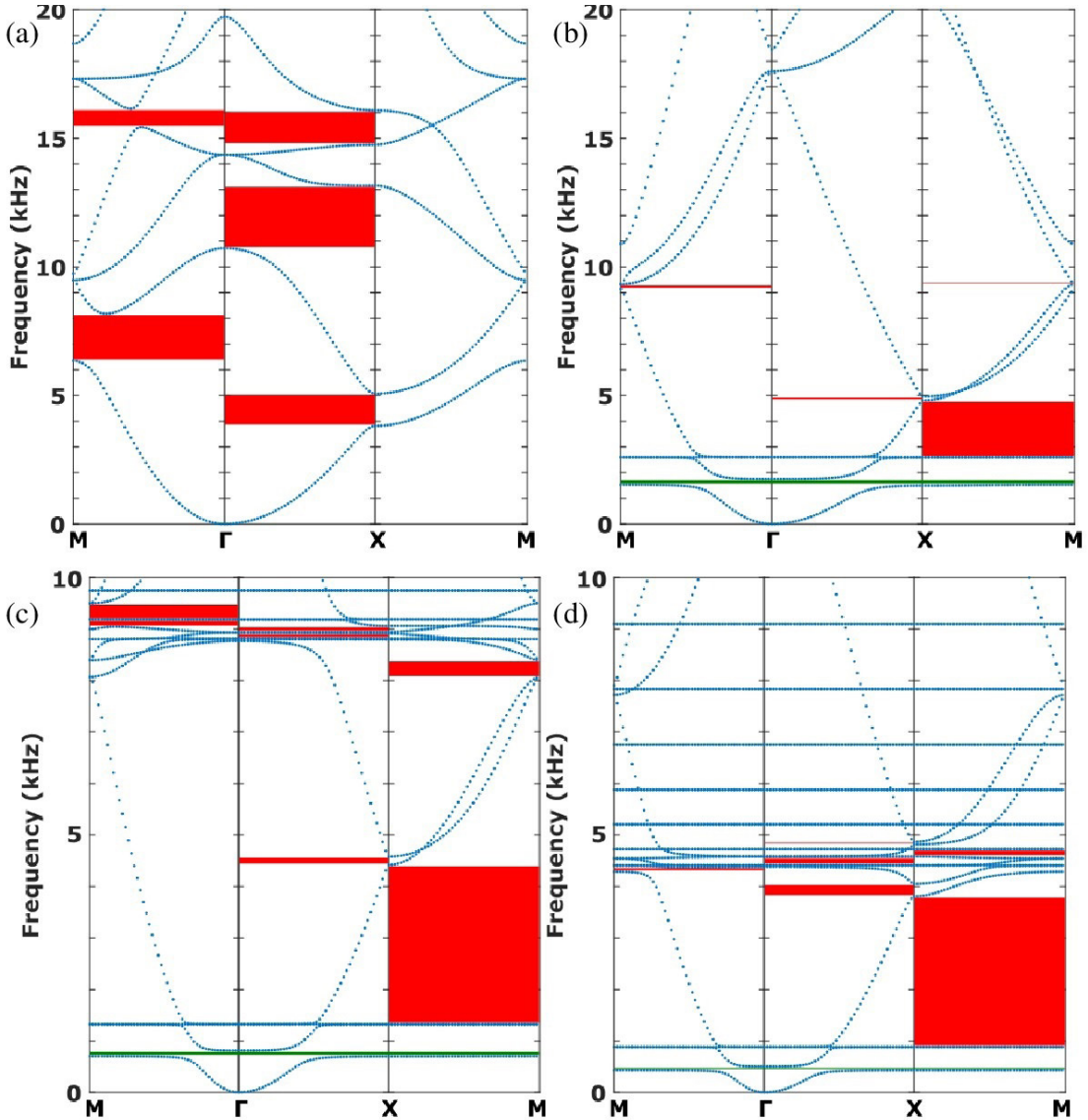
To investigate the effect of coating thickness on the flexural bandgaps, resonant aggregates with a fixed core diameter of 9 mm but varying coating thicknesses from 0.5 mm (T1) to 5 mm (T4), again, regarding the granulometry of coarse aggregate used civil construction. The geometric constants used in the simulation are given in Table 3.

Figure 6 illustrates the dispersion relations regarding the effect of coating thickness. As shown in Figure 6a, for a 0.5 mm coating (T1), there is no formation of complete

bandgaps, only partials, in M- $\Gamma$  and  $\Gamma$ -X directions. As the coating thickness increases (Figure 6b, T2), the partial bandgaps narrow, opening up bandgaps in X-M direction. Furthermore, a complete bandgap is formed between the frequencies from 1.53 to 1.75 kHz. With increasing coating thickness (Figures 6c, d, T3-T4), the absolute bandgap tends to shift to lower frequencies and narrows (within frequency range of 704-811 Hz and 430-506 Hz, respectively). This effect rises from the increase in the filling fractions of the compliant coating, which reduces the coating stiffness and, consequently, the global stiffness of system<sup>12</sup>. Furthermore, one can observe the formation of flatbands in the last two thicknesses, regions where there is no dispersion, *i.e.*, the energy is localized and it is not transported (zero group velocity), and extends along the entire IBZ, corresponding to the localized modes of the resonators, without bandgaps<sup>41</sup>. In Figure 6c (T3), flatbands appear at 1.32, 8.80, 9.18, and 9.75 kHz, while in Figure 6d (T4), occur at 0.88, 4.41, 4.58, 4.72, 5.21, 5.88, 6.75, 7.83, and 9.10 kHz. Therefore, the formation of flatbands is sensitive to the coating thickness.

**Table 3.** Resonator geometric data for effect of coating thickness.

ID	Core material	Coating material	Core diameter (mm)	Coating thickness (mm)	Resonator diameter (mm)
T1	Steel	Silicone	9	0.5	10
T2				2	13
T3				3.5	16
T4				5	19

**Figure 6.** Dispersion relation of a thin plate of metaconcrete containing steel resonators coated with silicone in configuration T1 (a), T2 (b), T3 (c), and T4 (d).

### 3.1.2. Study of material parameters

#### 3.1.2.1. Effect of core density

In order to evaluate the effect of the variation of the core density (considering the silicone as coating), four core materials are considered, fixing the geometric constants of the D4 configuration to investigate the second complete

bandgap. Table 4 summarizes the geometric and material properties used in the simulation.

Figure 7 presents the band structure for a metaconcrete thin plate containing different core densities. As seen in Figure 7a (AS, see Table 4), the complete bandgaps formed for the case of steel core (Figure 5d, D4 configuration) disappear, and only partial bandgaps were opened up.

This behavior arises from the reduction of the core density (aluminum), close to the density of concrete (2,730 and 2,500 kg/m<sup>3</sup>, respectively), providing a low contrast of the elastic parameters and, consequently, affecting the flexural performance of the metaconcrete. As aforementioned, using steel as the core material (Figure 7b, *i.e.*, SS, which is equal to the Figure 5d for D4 configuration), opens up two absolute bandgaps, due to the increase in material density and the contrast of elastic parameters. Replacing the steel core by copper (Figure 7c, CS), which has a higher density, the complete bandgaps shift to lower frequencies, widening (in the bandwidth from 2.55 to 3.06 kHz and from 3.97 to 4.22 kHz).

This behavior originates from the increase of mass contrast ratio between the aggregates and the matrix, broadening the region of negative effective mass density<sup>16</sup>. Lastly, the lead core was investigated (Figure 7d, LS), metal with the highest density used in this study. In this configuration, one can note that the complete bandgaps shift to lower frequencies and occupy a larger frequency range (from 2.23 to 2.79 kHz and from 3.51 to 3.96 kHz) in comparison to other metals, again, due to broadening the region of negative effective mass density. However, it is worth noting that the use of excessive dense core can be harmful, because the vibration of very heavy core might not be fully activated<sup>17</sup>.

**Table 4.** Resonator geometric and material properties for effect of core density.

ID	Core material	Coating material	Coating thickness (mm)	Core diameter (mm)
AS	Aluminum	Silicone	1	17
SS	Steel			
CS	Copper			
LS	Lead			

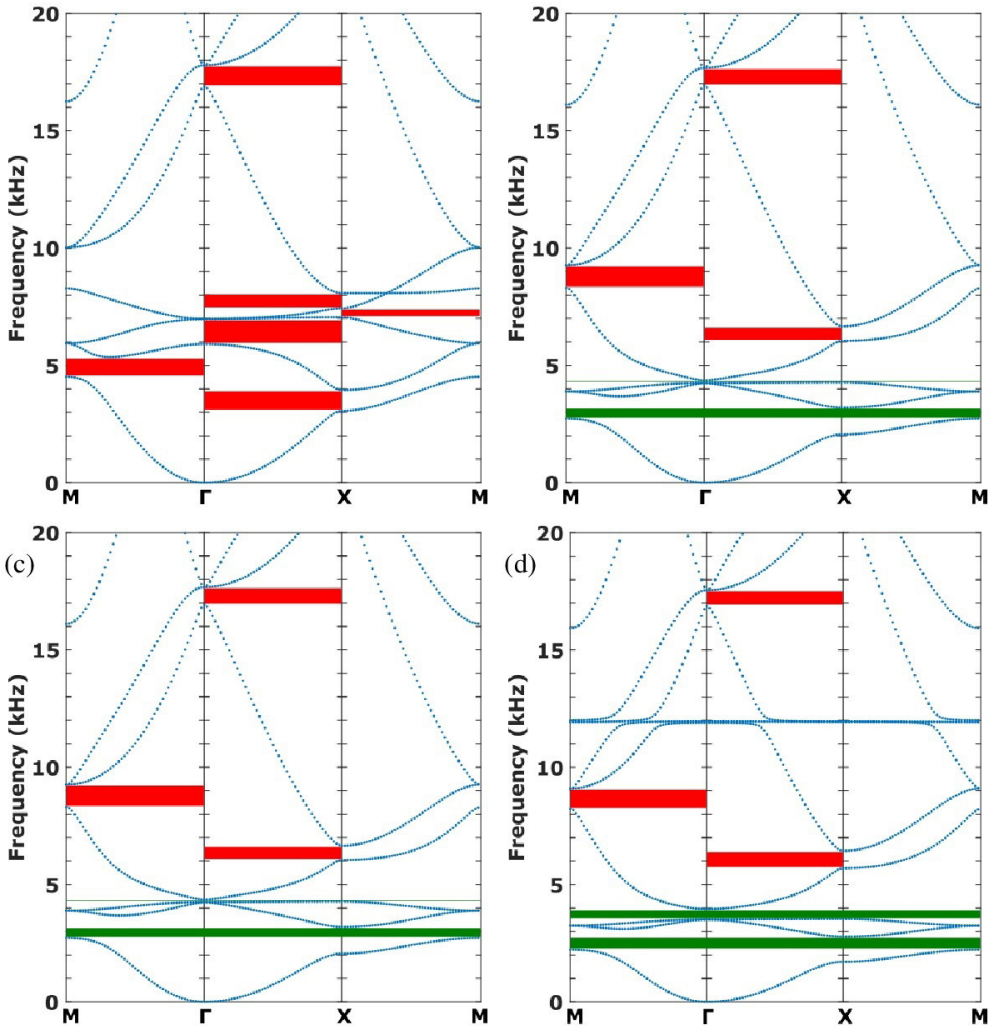


**Figure 7.** Dispersion relation of a thin plate of metaconcrete varying the core density in configuration AS (a), SS (b), CS (c), and LS (d).

### 3.1.2.2. Effect of coating stiffness

To verify the effect of the variation of the coating stiffness, four coating materials are considered, fixing the geometric data of the T2 configuration due to the larger bandgap. Table 5 lists the geometric and material properties used in the simulation.

In Figure 8, we illustrate the dispersion relation of a metaconcrete thin plate containing different coating stiffness. As can be noticed in Figure 8a (SS, see Table 5, which is equal to the Figure 6b for T2 configuration), the use of silicone, the softer coating material, produced a bandgap within frequency range of 1.53-1.75 kHz.

Increasing coating stiffness (Figure 8b, SR), leads to the widening of the bandgap and shifts it to the higher frequencies (from 4.27 to 4.80 kHz). This behavior arises from the increasing in coating stiffness, which must be stiff enough to allow energy transfer from the matrix to the core<sup>12</sup>. However, when excessively stiffness coatings are used (Figures 8c, d, SP-SN configurations), it can be seen that no complete bandgaps are formed up to the frequency of 20 kHz, opening up only partial bandgaps. Therefore, although increasing the coating stiffness enhances the performance of resonator, the use of materials with high Young's modulus can inhibit the core vibration in the dynamic process of metaconcrete<sup>16,17</sup>.

**Table 5.** Resonator geometric and material properties for effect of coating stiffness.

ID	Coating material	Core material	Coating thickness (mm)	Core diameter (mm)
SS	Silicone	Steel	2	9
SR	Natural rubber			
SP	LPDE			
SN	Nylon			

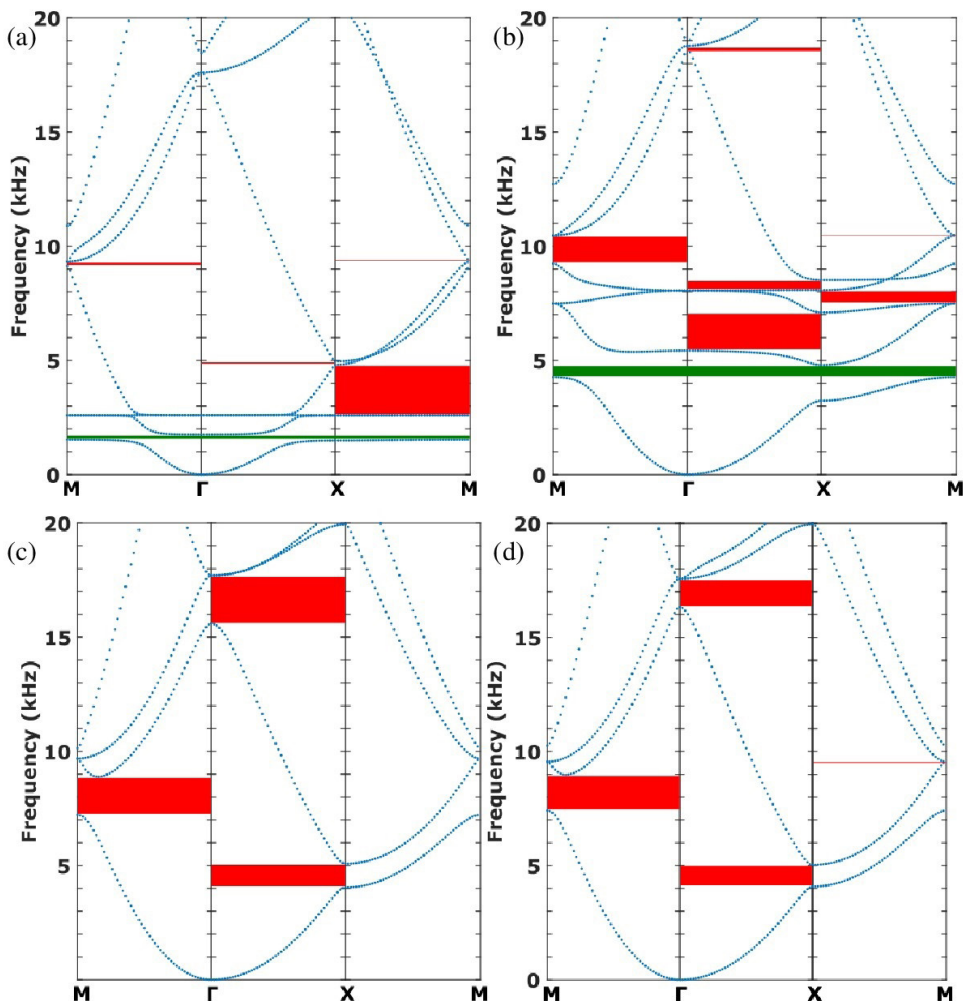


**Figure 8.** Dispersion relation of a thin plate of metaconcrete varying the coating stiffness in configuration SS (a), SR (b), SP (c), SN (d).



### 3.2. Metaconcrete containing multi-layer resonator

In this section, a novel resonant aggregate is proposed, known as multilayer aggregate. To study the effect of number of layers on the flexural bandgaps, we provide a numerical investigation of this new resonator. To this end, we have maintained the total diameter at 19 mm, spreading the coating and core into distinct layers – metallic layers named as core and cover (light gray regions in Figure 3b), while the polymeric layers were called coating and shell (white regions in Figure 3b). The material and structural parameters of the IPWE model are displayed in Tables 6 and 7, respectively.

Figures 9-11 show the bandgap widths (in Hz) and midgap frequencies (in kHz) of the first three complete bandgaps, respectively, for all configurations considered. Firstly, one can note in Figure 9 that the ASAS configuration (see Table 6), made of aluminum/silicone, presents an absolute bandgap, in contrast with AS single-layer resonator (Figure 7a) with the same total diameter. In addition, the flexural bandgaps are sensitive to number of layers, since the bandgap width augmented for all configurations in comparison to the single-layer counterparts. By way of example, the biggest increase occurs when using lead and the first complete bandgap of the multilayer resonator (LSLS in Figure 9) increases by up to 34% compared to the single-layer inclusion (Figure 7d). However, the upper limit frequency drops slower than the lower limit frequency. Moreover, as noted for single-layer inclusion, the increasing in core/cover density leads to a widening in frequency range and shifts the complete bandgap to lower frequencies.

As illustrated in Figure 10, even a second complete bandgap was opened up in the ASAS configuration. Once more, using the multilayer resonator (Figure 10) widens the second bandgap width for all configurations in comparison to the single-layer counterparts (Figure 7). Nevertheless, the core/cover density seems to restrict this behavior to the second complete bandgap, whereas the biggest rise was observed in SSSS configuration, around 222%, and the LSLS showed the smallest increase, around 11%. Furthermore, both lower and upper limit frequencies of the second absolute bandgap shift to the higher frequencies at a faster rate than the first complete bandgap.

Lastly, Figure 11 shows that a narrow third complete bandgap, at higher frequency, was opened up in the LSLS configuration. Since LSLS configuration displayed the smallest bandwidth increase ratio and a third complete bandgap, since increasing the core/cover density transfers portion of the energy required to open up the absolute bandgap to a higher frequencies in the multilayer resonator.

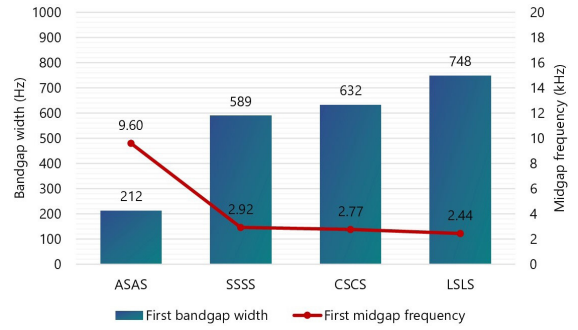


**Figure 9.** Bandgap widths (Hz) and midgap frequencies (kHz) for the first complete bandgap for ASAS, SSSS, CSCS and LSLS configurations.

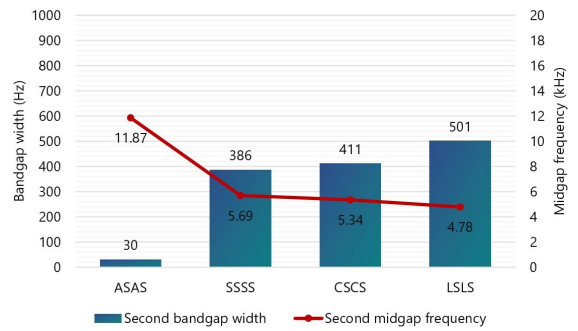


**Figure 10.** Bandgap widths (Hz) and midgap frequencies (kHz) for the second complete bandgap for ASAS, SSSS, CSCS and LSLS configurations.

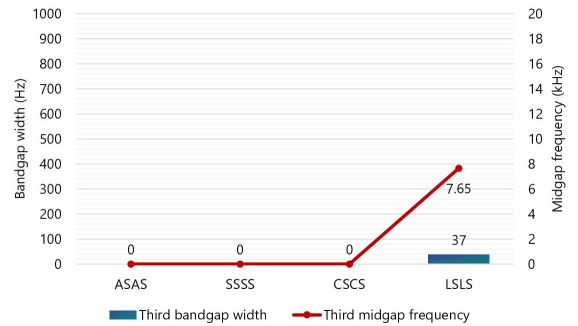


**Figure 11.** Bandgap widths (Hz) and midgap frequencies (kHz) for the third complete bandgap for ASAS, SSSS, CSCS and LSLS configurations.

**Table 6.** Material parameters of multilayer resonator.

ID	Core material	Coating material	Cover material	Shell material
ASAS	Aluminum	Silicone	Aluminum	Silicone
SSSS	Steel		Steel	
CSCS	Copper		Copper	
LSLS	Lead		Lead	

**Table 7.** Geometric data of multilayer resonator.

Core diameter (mm)	Coating thickness (mm)	Cover thickness (mm)	Shell thickness (mm)	Total diameter (mm)
8	1	3.5	1	19

## 4. Conclusions

Recently, the metamaterials concept has been introduced in civil construction. Called metaconcrete, this new type of concrete can be designed to prevent or reduce elastic waves from propagating in specified frequencies, due to regions termed as bandgaps. In this study, a computational numerical analysis was carried out, evaluating the effect of core diameter, coating thickness, core density, and coating stiffness of circular resonators arranged in a square array on flexural bandgap formation of a metaconcrete thin plate, using the Kirchhoff-Love plate theory. Furthermore, a novel multilayer resonator was developed.

In the numerical calculations, we do not observe the formation of bandgaps in the ordinary concrete band structure considering the frequency range of this study, so it is not capable of reducing the vibration of elastic waves through resonance and Bragg scattering mechanisms. In the analyzed core sizes and coating thickness cases, bandgap width and location are sensitive to these parameters. Increasing core diameter initially widens the bandgap region, but use of large diameters can cause greater resistance to core vibration, narrowing the negative effective mass density region. On the other hand, the core size enhancement opens up a second absolute bandgap. The increase of coating thickness narrows the bandgap region, which shifts to lower frequencies. Furthermore, this material parameter controls the flatbands mechanism, which occurs in thicker coatings.

The results with respect to core density and coating stiffness variability show that location, width and even formation of the bandgap frequency are highly sensitive to these parameters. When using metals with a density close to that concrete, the contrast of the elastic properties is insufficiently different to open complete bandgaps in the range investigated. Complete bandgaps were opened up with increasing the core density, which raise the mass contrast ratio between resonators and matrix. Increasing stiffness coating shifts the complete bandgap to higher frequency ranges, widening it. However, using too stiff coating can affect core vibration, as observed for LPDE and nylon (*i.e.*, the two most rigid coatings used in simulations), complete bandgaps are not opened up within the frequency range investigated.

It is also found the possibility of design multilayer resonant aggregates to optimize the flexural band structure. Multilayer resonator bandgaps were more prominent than the single-layer counterparts were and, even when used a metal with density close to the concrete, bandgaps were opened up. Therefore, the materials setting in different layers remarkably influence the metaconcrete performance.

The work proposes an efficient flexural vibration management through metaconcrete thin plate, with tunable properties of resonant single- and multilayer aggregates, covering wider frequencies in the sonic range ( $f \leq 20$  kHz).

Future works should investigate the influence of unit cell size, plate thickness, geometry of resonators and lattice type for optimizing the bandgap formation to control flexural vibration in low frequencies and the possibility of taking advantage of presence of flatbands in softer thick coatings.

## 5. Acknowledgments

The authors thank the Instituto Federal do Maranhão (IFMA), Brazilian funding agencies CAPES (Finance Code 001), CNPq (Grant Reference Numbers 317436/2021-0, 403234/2021-2, 405638/2022-1, and 300166/2022-2), FAPEMA (Grant Reference Numbers BM-05441/19, and BM-07223/22), and FAPESP (Grant Reference Number 2018/15894-0).

## 6. References

- Joannopoulos JD, Johnson SG, Winn JN, Meade RD. Photonic crystals: molding the flow of light. 2nd ed. New Jersey: Princeton; 2008.
- Lu MH, Feng L, Chen YF. Phononic crystals and acoustic metamaterials. *Mater Today*. 2009;12(12):34-42.
- Pennec Y, Vasseur JO, Djafari-Rouhani B, Dobrzyński L, Deymier PA. Two-dimensional phononic crystals: Examples and applications. *Surf Sci Rep*. 2010;65(8):229-91.
- Lee JH, Koh CY, Singer JP, Jeon SJ, Maldovan M, Stein O, et al. 25th anniversary article: Ordered polymer structures for the engineering of photons and phonons. *Adv Mater*. 2014;26(4):532-69.
- Liu Z, Zhang X, Mao Y, Zhu YY, Yang Z, Chan CT, et al. Locally resonant sonic materials. *Science*. 2000;289(5485):1734-6.
- Oh JH, Kwon YE, Lee HJ, Kim YY. Elastic metamaterials for independent realization of negativity in density and stiffness. *Sci Rep*. 2016;6:1-10.
- Zheng X, Guo X, Watanabe I. A mathematically defined 3D auxetic metamaterial with tunable mechanical and conduction properties. *Mater Des*. 2021;198:109313.
- Wu W, Liu P, Kang Z. A novel mechanical metamaterial with simultaneous stretching- and compression-expanding property. *Mater Des*. 2021;208:109930.
- Wenz F, Schmidt I, Lechner A, Licht T, Baumann S, Andrae H, et al. Designing shape morphing behavior through local programming of mechanical metamaterials. *Adv Mater*. 2021;33(37):2008617.
- Wu L, Wang Y, Zhai Z, Yang Y, Krishnaraju D, Lu J, et al. Mechanical metamaterials for full-band mechanical wave shielding. *Appl Mater Today*. 2020;20:100671.
- Coulais C, Sounas D, Alù A. Static non-reciprocity in mechanical metamaterials. *Nature*. 2017;542(7642):461-4.
- Mitchell SJ, Pandolfi A, Ortiz M. Metaconcrete: Designed aggregates to enhance dynamic performance. *J Mech Phys Solids*. 2014;65(1):69-81.
- Oyelade AO, Sadiq MO, Abiodun YO. Dynamic behaviour of concrete containing aggregate resonant frequency. *J Comput Appl Mech*. 2018;49(2):380-5.
- Kettenbeil C, Ravichandran G. Experimental investigation of the dynamic behavior of metaconcrete. *Int J Impact Eng*. 2018;111:199-207.
- Tan SH, Poh LH, Tkalic D. Homogenized enriched model for blast wave propagation in metaconcrete with viscoelastic compliant layer. *Int J Numer Methods Eng*. 2019;119(13):1395-418.
- Xu C, Chen W, Hao H. The influence of design parameters of engineered aggregate in metaconcrete on bandgap region. *J Mech Phys Solids*. 2020;139:103929.
- Xu C, Chen W, Hao H, Jin H. Effect of engineered aggregate configuration and design on stress wave attenuation of metaconcrete rod structure. *Int J Solids Struct*. 2021;232:111182.
- Han J, Lu G. A study of undamped free vibration characteristics on a metaconcrete unit cell. *J Vib Shock*. 2021;40(8):173-8.
- Briccola D, Cadoni E. Split Hopkinson bar tests on metaconcrete: Modeling and numerical simulations. *EPJ Web Conf*. 2021;250:1-9.

20. Briccola D, Tomasin M, Netti T, Pandolfi A. The influence of a lattice-like pattern of inclusions on the attenuation properties of metaconcrete. *Front Mater.* 2019;6:1-9.
21. Xu C, Chen W, Hao H, Pham TM, Bi K. Damping properties and dynamic responses of metaconcrete beam structures subjected to transverse loading. *Constr Build Mater.* 2021;311:125273.
22. Xu C, Chen W, Hao H, Bi K, Pham TM. Experimental and numerical assessment of stress wave attenuation of metaconcrete rods subjected to impulsive loads. *Int J Impact Eng.* 2022;159:104052.
23. Briccola D, Ortiz M, Pandolfi A. Experimental validation of metaconcrete blast mitigation properties. *J Appl Mech.* 2017;84(3):2-7.
24. Briccola D, Cuni M, De Juli A, Ortiz M, Pandolfi A. Experimental validation of the attenuation properties in the sonic range of metaconcrete containing two types of resonant inclusions. *Exp Mech.* 2021;61(3):515-32.
25. Briccola D, Pandolfi A. Analysis on the dynamic wave attenuation properties of metaconcrete considering a quasi-random arrangement of inclusions. *Front Mater.* 2021;7:1-14.
26. Ru C. A simplified metaelastic model for coated sphere-filled random composites. *Math Mech Solids.* 2021;26(7):939-53.
27. Liu Y, An X, Chen H, Fan H. Vibration attenuation of finite-size metaconcrete: Mechanism, prediction and verification. *Compos, Part A Appl Sci Manuf.* 2021;143:106294.
28. Cuenca J. Wave models for the flexural vibrations of thin plates: Model of the vibrations of polygonal plates by the image source method - vibration damping using the acoustic black hole effect [thesis]. Le Mans, France: Université du Maine; 2009.
29. Dian-Long Y, Gang W, Yao-Zong L, Ji-Hong W, Jing Q. Flexural vibration band gaps in thin plates with two-dimensional binary locally resonant structures. *Chin Phys.* 2006;15(2):266-71.
30. Wang T, Sheng MP, Guo ZW, Qin QH. Flexural wave suppression by an acoustic metamaterial plate. *Appl Acoust.* 2016;114:118-24.
31. Zouari S, Brocaïl J, Gènevaux JM. Flexural wave band gaps in metamaterial plates: a numerical and experimental study from infinite to finite models. *J Sound Vibrat.* 2018;435:246-63.
32. Chen X, Cai L, Wen JH. Controlling flexural waves in thin plates by using transformation acoustic metamaterials. *Chin Phys B.* 2018;27(5):057803.
33. Miranda Jr. EJP, Angelin AF, Silva FM, Santos JMC. Passive vibration control using a metaconcrete thin plate. *Cerâmica.* 2019;65(Suppl. 1):27-33.
34. Yao ZJ, Yu GL, Wang YS, Shi ZF. Propagation of bending waves in phononic crystal thin plates with a point defect. *Int J Solids Struct.* 2009;46(13):2571-6.
35. Barnwell EG, Parnell WJ, Abrahams ID. Tunable elastodynamic band gaps. *Extreme Mech Lett.* 2017;12:23-9.
36. Dal Poggetto VF, Serpa AL. Flexural wave band gaps in a ternary periodic metamaterial plate using the plane wave expansion method. *J Sound Vibrat.* 2021;495:115909.
37. Mehta PK, Monteiro PJM. *Concreto: Microestrutura, propriedades e materiais.* 2ª ed. São Paulo: IBRACON; 2014. [Portuguese].
38. Qian D, Shi Z. Using PWE/FE method to calculate the band structures of the semi-infinite beam-like PCs: Periodic in z-direction and finite in x-y plane. *Phys Lett A.* 2017;381(17):1516-24.
39. Callister WD, Rethwisch DG. *Ciência e engenharia de materiais: Uma introdução.* 8ª ed. Rio de Janeiro: LTC; 2012. [Portuguese].
40. Bauer LAF. *Materiais de construção.* 6ª ed. Rio de Janeiro: LTC; 2019. [Portuguese].
41. Ma TX, Fan QS, Zhang C, Wang YS. Acoustic flatbands in phononic crystal defect lattices. *J Appl Phys.* 2021;129(14):145104.